Supplement of Geosci. Model Dev., 13, 507–520, 2020
https://doi.org/10.5194/gmd-13-507-2020-supplement
© Author(s) 2020. This work is distributed under
the Creative Commons Attribution 4.0 License.

Geoscientific
Model Development
Open Access

Supplement of

ORCHIDEE MICT-LEAK (r5459), a global model for the production, transport, and transformation of dissolved organic carbon from Arctic permafrost regions – Part 2: Model evaluation over the Lena River basin

Simon P. K. Bowring et al.

Correspondence to: Simon P. K. Bowring (simon.bowring@lsce.ipsl.fr)

The copyright of individual parts of the supplement might differ from the CC BY 4.0 License.

Text S1: Evaluation of Simulated NPP and Soil Respiration

Rates of yearly net primary production (NPP) for Russian and Siberian forests have been inferred in situ from eddy flux and inventory techniques to range from 123-250 gC m^{-2} yr^{-1} (Beer et al., 2006; Lloyd et al., 2002; Roser et al., 2002; Schulze et al., 1999; Shvidenko and Nilsson, 2003). We likewise simulate a broad range of NPP carbon uptake rates, of 61-469 gC m^{-2} yr^{-1} averaged per grid cell over the Lena basin, with a mean value of 210 gC m^{-2} yr^{-1}. NPP is heterogeneously distributed over space and between PFTs (SI, Fig. S4c), with forests averaging 90 gC m^{-2} yr-^{1} and grasslands averaging 104 gC m^{-2} yr-^{1} over the basin as a whole. Low values tended to originate in basin grid cells with elevated topography or high mean slope, while the maximum value was standalone, exceeding the next greatest by ~100 gC m^{-2} yr^{-1}, and is most likely caused by the edge effects of upscaling a coastal gridcell's small fraction of terrestrial area where high productivity occurs in a small plot, to the grid cell as a whole. By evaluating NPP we are also evaluating at a secondary level litter production, which is at a third level a major component of DOC production.

Taken as a whole, gross primary production (GPP) was performed under simulations by four PFT groups, with the largest basin-wide bulk contributions coming from boreal needleleaf summer-green trees and C3 grasses (SI, Fig. S4a), the highest GPP uptake rates (3 TgC pixel^{-1} yr^{-1}) generated by boreal needleleaf evergreen trees, and the remainder of GPP contributed by Boreal broad-leaved summer-green trees (SI, Fig. S4a).

Soil respiration rates, of combined soil heterotroph and plant root respiration in our Control simulation, averaged 208 gC m^{-2} yr^{-1} (0.57 gC m^{-2} d^{-1}) over the Lena basin over the period 1990-2000, which is somewhat higher than those found by Elberling (2007) in tundra soils over Svalbard, of 103-176 gC m^{-2} yr^{-1} (0.28-0.48 gC m^{-2} d^{-1}). Sawamoto, et al. (2000) measured in situ summertime soil respiration over the central Lena basin and found rates of 1.6-34 gC m^{-2} d^{-1}, while Sommerkorn (2008) observed rates of 0.1-3.9 gC m^{-2} d^{-1} at higher latitudes, these appearing to vary with vegetation and fire history, water table depth and temperature. Mean heterotrophic respiration rates of 1.6 gC m^{-2} d^{-1} are simulated here during July and August, in the range 0.0.5-2.2 gC m^{-2} d^{-1} for each of the above PFT groups. The spatial distribution of, and difference in respiration rates between PFT groups largely mirrors those for NPP (SI Fig. S4c), with maximum rates of 1.4 gC m^{2} d^{-1} over forested sites, versus a maximum of 2.2 gC m^{2} d^{-1} over grassland/tundra sites (SI, Fig. S4b).

Aggregated over the basin, results show that increases over the course of the 20th Century were simulated for NPP, GPP, River Discharge, DOC, $CO_{2(aq.)}$, autotrophic and heterotrophic respiration and CO_2 evasion, with percentage changes in the last versus first decade of +25%, +27%, 38%, +73%, +60%, +30%, +33% and +63%, respectively. (Fig. S12). It thus appears that rising temperatures and CO_2 concentrations disproportionately favoured the metabolisation of carbon within the soil and its transport and mineralisation within the water column, fed by higher rates of primary production and litter formation as well as an accelerated hydrological cycle.

Text S2: Deficiencies in Modelled Hydrology

Deficiencies in modelled hydrology correspond to those found in Fig. 12 of Guimberteau et al. (2018), indicating that the modifications made in this model version, which focus on the DOC cycle, have not further degraded the hydrological performance of the model, the causes of which are described below. Low simulated discharge for the Lena basin, particularly during the late summer and autumn, is consistent with prior, Pan-Arctic simulations conducted by Guimberteau et al. (2018), who ran ORCHIDEE-MICT using both the GSWP3 and CRU-NCEP v7 datasets and evaluated them over the period 1981-2007. Despite the substantially better hydrological performance of ORCHIDEE under GSWP3 climate, they described a near-systematic underestimation of summer/autumn discharge rates for both datasets over the Yukon, Mackenzie, Lena and Kolyma basins. Furthermore, the discrepancy of model output between climatological datasets was almost as large as the discrepancy between model output and observational data in that study, which analysed this in great depth, suggesting that the source of error is both a covariate of model process representation and parameterisation, as well as the climatological datasets themselves. Model hydrological representation and empirically derived climate input data are then subject to interaction with modelled soil (e.g. infiltration), vegetation (e.g. canopy interception) and thermodynamics (e.g. freezing and consequent partitioning of water transport) from which river discharge is computed, confounding full interpretation of sources of bias, briefly described below.

Model process deficiency in this regard was identified by Guimberteau et al. (2018) as residing in an overly restrictive representation of water impermeability through frozen topsoil, which decreases the residence time of running water by directing it to surface runoff rather than subsurface flow, and in the process increases the susceptibility of the total water volume to evapotranspiration from incoming shortwave radiation. This would bias both the timing (over-partitioning of water to high runoff periods) and volume of water (low bias) reaching the river stem and its eventual discharge into the ocean, respectively, as demonstrated by model output. Guimberteau et al. (2018) suggest that representation of sub-grid-scale infiltration mechanisms under frozen conditions, such as soil freezing-drying that would enhance infiltration, be included in future, yet-to-be implemented iterations of ORCHIDEE. Furthermore, we suggest that the lack of representation of lakes in ORCHIDEE, which serve to increase the time lag between precipitation/melt and oceanic discharge, may likewise be a powerful source of bias in the timing of discharge fluxes represented by the model.

Unsurprisingly, simulated surface runoff has been shown to be strongly affected by differences in precipitation between datasets (Biancamaria et al., 2009; Fekete et al., 2004), while biases in these and evapotranspiration datasets that are used to both drive and evaluate the hydrological models, are a powerful source of water balance biases in high-latitude basins (Wang et al., 2015). Indeed, climatological dataset estimates for the spatial distribution of high latitude winter snowfall are generally problematic, owing to the low density of meteorological stations (Burke et al., 2013), wind-related issues with in-field collection and measurement that lead to systematic underestimates of snowfall rates (Yang et al., 2005), creating biases in the climatological datasets that only show up when the integrator of their model input -in this case river discharge -is modelled. In addition, the wintertime partitioning of precipitation between rain and snow, a function of 2m air temperatures in the forcing datasets, strongly affects the volume and timing of runoff (Guimberteau et al., 2018; Haddeland et al., 2011). Indeed, 69% of the spatial variance of the spring freshet has been attributed to snow water-equivalent bias during the pre-melt season (Rawlins et al., 2007). In addition, errors in forcing of soil evaporation due to inaccuracies in incoming shortwave radiation, as well as biases in the parameterisation of canopy interception -a function of simulated LAI -can lead to upward biases in evapotranspiration rates (Guimberteau et al., 2018).

Text S3: Deficiencies in Modelled DOC Discharge

Firstly, there is a quasi-linear positive relationship between DOC discharge and river discharge (Fig. 3d). This relation is common to Arctic rivers, as DOC loading experiences disproportionately large increases with increases in discharge (Fig. 4, Raymond et al., 2007), owing largely to the 'flushing' out of terrestrially fixed carbon from the previous year's production by the massive runoff generated by ice and snow melt during the spring thaw. Comparing simulated annual mean discharge rate ($m^3\ s^{-1}$) with long-term observations (Ye et al. 2003) over years 1940-2000 (Fig. S3) shows that though absolute discharge rates are underestimated by simulations, their interannual variation reasonably tracks the direction and magnitude of observations. Linear regressions through each trend yield very similar yearly increases of 29 vs 38 $m^3\ s^{-1}\ yr^{-1}$ for simulations and observations, respectively. The observed vs. simulated mean annual water discharge differential hovers at 36% (Figs. 3d, 4c), close to the 43% differential between observed and simulated DOC discharge, giving some indication that, given the linear relationship between water and DOC discharge, most of the DOC discrepancy can be explained by the performance of the hydrology and not the DOC module, the latter of which was the subject of developments added in ORCHIDEE M-L. Applying the regression slope of the relationship in Fig. 3d (9E-06 mgC per $m^3 s^{-1}$) to the mean river discharge discrepancy of 36%, we find that 84% of the differential between observed and simulated discharge can be explained by the underperformance of the hydrology module.

Further sources of error are process exclusion and representation/forcing limitations. Indeed, separate test runs carried out using a different set of climatological input forcing show that changing from the GSWP3 input dataset to input from bias-corrected projections from the IPSL Earth System Model under the second Inter-Sectoral Impact Model Intercomparison Project (ISIMIP2b (Frieler et al., 2017; Lange, 2016, 2018)) protocol increases DOC discharge to the ocean to 4.14 TgC yr^{-1} (+37%), largely due to somewhat higher precipitation rates in that forcing dataset (see Table S3). Thus, the choice of input dataset itself introduces a significant degree of uncertainty to model output.

In addition, this model does not include explicit peatland formation and related dynamics, which is the subject of further model developments (Qiu et al., 2018) yet to be included in this iteration. With peatlands thought to cover ~17% of the Arctic land surface (Tarnocai et al., 2009), and with substantially higher leaching concentrations, this may be a significant omission from our model. The remaining biases likely arise from errors in the interaction of simulated NPP, respiration and DOC production and decomposition, which will impact on the net in and out -flow of dissolved carbon to the fluvial system. However, the DOC relationship with these variables is less clear-cut than with river discharge. Indeed, regressions (Fig. S2) of annual DOC versus NPP (TgC yr^{-1})

show that DOC is highly sensitive to increases in NPP, but is less coupled to it (more scattered, $R^2=0.42$) than other simulated fluvial carbon variables shown, i.e. aquatic CO_2 evasion and soil CO_2 export to the river network. The differences in correlation and slope of the variables in Fig. S2 are expected: aquatic CO_2 evasion is least sensitive yet most tightly coupled to NPP ($R^2=0.52$), while CO_2 export to rivers is intermediate between the two ($R^2=0.43$). The greater correlation with NPP of DOC compared to evasion is understandable, given that DOC leaching is a covariate of both NPP and runoff, whereas evasion flux is largely dependent on organic inputs (production) and temperature (see Part 1).

Text S4: Model Evaluation: DOC Discharge Seasonality

Figure 4b shows that the bulk of the DOC outflow occurs during the spring freshet, accounting for ~50-70% of the total Arctic outflow (Lammers et al., 2001; Ye et al., 2009), in which DOC concentrations increase, as meltwater flushes out DOC accumulated from the previous year's litter and SOC generation (Raymond et al., 2007; Kutscher et al., 2017), reproduced in Fig. 4b. Simulation of the hydrological dynamic is presented in maps of river discharge through the basin in Fig. 3b, which show low-flows in April with substantial hydrographic flow from upstream mountainous headwaters and Lake Baikal inflow in the south, peak flow in June dominated by headwaters, and little headwater input in September.

In Fig. 4b we observe the following: (i) DOC discharge fluxes closely track hydrological fluxes. (ii) The simulated modern river discharge peak approximates the historical observed discharge peak, but slightly overestimates spring fluxes and substantially underestimates fluxes in the autumn, as explained above. (iii) The difference between the first and last decades of the simulation in Fig. 4b is mostly attributable to a large increase in the DOC flux mobilised by spring freshet waters. This suggests both greater peaks in simulated DOC flux and a shift to earlier peak timing, owing to an increase in river discharge, indicative of an earlier spring and a progressively warmer environment over the 20th Century. (iv) The maximum modelled modern monthly DOC flux rate of ~1.3 TgC month^{-1} is comparable to the mean maximum DOC flux rate measured in a recent study (1.75 TgC month^{-1}, Kutscher et al., 2017, Fig. 2).

We compare the Raymond et al. (2007) modern DOC outflow (Fig. 4d, solid black line) against simulated DOC outflow from both Zhigansk and Kusur (Fig. 4d). Simulated DOC flux is underestimated for both sites. Peakflow at Zhigansk seems to be attenuated over May and June in simulations, as opposed to May peakflow in observations. Peakflow at Kusur is definitively in June. This suggests that simulated outflow timing at Zhigansk may slightly delayed, causing a split in peak discharge when averaged in the model output. Thus the aggregation of model output to monthly averages from calculated daily and 30 minute timesteps can result in the artificial imposition of a normative temporal boundary (i.e. month) on a continuous series. This may cause the less distinctive 'sharp' peak seen in Fig. 4c, which is instead simulated at the downstream Kusur site, whose distance some 500km away from Zhigansk more clearly explains the delay difference in seasonality. We further evaluate our DOC discharge at the sub-basin scale, to test whether the fractional contribution of different DOC flows from each sub-basin correspond to those in their observed correlates from Kutscher et al., (2017). This comparison is depicted in Fig. S5, where the observed and simulated percentage DOC contributions of the Aldan, Vilui, and Upper and Lower Lena sub-basins to total flux rates are 19 (24)%, 20(10%), 33 (38%) and 30 (28)% in simulations (observations) for the four sub-basins, respectively. While deviations between simulated and observed DOC fluxes can be expected, the nearly twofold value mismatch of the Vilui basin is due to its real-word damming, not represented here. On the other hand, we cannot explain the ~5% discrepancies in other sub-basin fluxes, particularly for the Aldan.

Text S5: Evaluation of Modelled DOC Concentrations in Stream, River, Ground Water

The spatial distribution of DOC concentrations are shown in maps of mean monthly DOC concentration for stream water, river water and groundwater (Fig. S6a,b,c, respectively) in April, June and September. For both the stream and river water reservoirs, DOC concentrations appear to have spatio-temporal gradients correlated with the flux of water over the basin during the thaw period, with high concentrations of 10-15 mgC L^{-1} driven by April meltwaters upstream of the basin, these high concentrations moving northward to the coldest downstream regions of the basin in June. Lower DOC concentrations of ~5 mgC L^{-1} dominate the basin in September when the bulk of simulated lateral flux of DOC has dissipated into the Laptev Sea. In contrast, groundwater DOC concentrations are generally stable with time, although some pixels appear to experience some 'recharge' in their concentrations during the first two of the three displayed thaw months. Significantly, highest groundwater DOC concentrations of up to 20 mgC L^{-1} are focussed on the highest elevation areas of the Lena basin on its Eastern boundary, which are characterized by a dominance of Podzols (SI, Fig. S9b). This region, the Verkhoyansk range, is clearly visible as the high groundwater DOC concentration (2-20mgC L^{-1}) arc (in red) in Fig. S6a, as well as other high elevation areas in the south-western portion of the basin (Fig. 3a), while the low-lying central basin shows much smaller groundwater DOC concentrations (0-2mgC L^{-1}). The range of simulated groundwater DOC concentration comes close to those aggregated from the empirical literature by Shvartsev (2008), which finds from >9,000 observations that groundwater in permafrost regions exhibit a mean concentration of ~10 mgC L^{-1} after peatlands and swamps (not simulated here) are removed (Table 2).

The high groundwater reservoir DOC concentrations simulated in high altitude regions by ORCHIDEE MICT-L is related to the fact that, in the model, DOC is rapidly produced and infiltrated deep into soil above the permafrost table, to the point that it reaches the simulated groundwater pool relatively quickly, allowing it to enter this reservoir before being metabolised through the soil column –hence allowing for the relatively high groundwater concentrations found in mountain areas. Because of the prevailing low temperatures, this DOC is not quickly decomposed by microbes and instead feed the groundwater DOC pool.

Text S6: Riverine CO_2 Evasion

In our model, the fate of DOC once it enters the fluvial system is either to remain as DOC and be exported to the ocean, or to be degraded to dissolved CO_2 ($CO_{2(aq.)}$), which is itself either also transported to the marine system or outgassed from the fluvial surface to the atmosphere (see Part 1, Section 2.10). The latter two outcomes also apply to $CO_{2(aq.)}$ produced in the soil by organic matter degradation and subsequently transported by runoff and drainage flows to the water column. As shown in Fig. 2, a large proportion of DOC (38%, 2.1 TgC yr^{-1}) that enters the water column is degraded to $CO_{2(aq.)}$ during transport, which adds to the 1.65 TgC yr-^{1} of direct $CO_{2(aq.)}$ input from the terrestrial land surface. Of this bulk CO_2 exported into and generated within the water column, 3.6 TgC yr^{-1} evades from the water surface to the atmosphere before reaching the river delta. In what follows, we evaluate first inputs of $CO_{2(aq.)}$ to the water column in terms of their seasonality, before evaluating CO_2 evasion rates and the relation of this to smaller and larger water bodies (river versus stream).

To our knowledge, no direct measurements for CO_2 evasion from the surface of the Lena river are available in the literature. We refer to Denfeld et al. (2013) for evaluating our evasion flux results, since their basin of study, the Kolyma River, is the most geographically proximate existing dataset to the Lena, despite biogeographical differences between the two basins –namely that the Kolyma is almost entirely underlain by continuous permafrost. The Kolyma River CO_2 evasion study measured evasion at 29 different sites along the river basin (~158-163°E; 68-69.5°N), with these sites distinguished from one another as 'main stem', 'inflowing river' or 'stream' on the basis of reach length. The study showed that during the summer low-flow period (August), areal river mainstem CO_2 evasion fluxes were ~0.35 gC m^{-2} d^{-1}, whereas for streams of stream order 1-3 (widths 1-19m), evasion fluxes were up to ~7 gC m^{-2} d^{-1}, and for non-mainstem rivers (widths 20-400m) mean net fluxes were roughly zero (Table 3 of Denfeld et al., 2013). Thus, while small streams have been observed to contribute to roughly 2% of the Kolyma basin surface area, their measured percentage contribution to total basin-wide CO_2 evasion ~40%, whereas for the main stem the surface area and evasion fractions were ~80% and 60%, respectively. Likewise, mean annual evasion rates of <0.8 up to around 7 gC m^{-2} d^{-1} have been found for the Ob and Pur rivers in Western Siberia (Serikova et al., 2018).

Results such as these, in addition to permafrost soil incubation experiments (e.g. Drake et al., 2015; Vonk et al., 2013, 2015b, 2015a) suggest that small streams, which represent the initial (headwater) drainage sites of these basins, rapidly process hydrologically leached carbon to the atmosphere, and that this high-reactivity carbon is a mix of recently thawed ancient permafrost material, as well as decomposing matter from the previous growth year. This is given as evidence that the total carbon processing of high-latitude rivers is significantly underestimated if only mainstem carbon concentrations are used in the accounting framework, since a large amount of carbon is metabolised to the atmosphere before reaching the site of measurement.

Text S7: Spatio-Temporal Heterogeneity in CO2 Evasion

The heterogeneity of CO_2 evasion from different sources in the model is most evident in terms of their geographic distribution and relative intensity, as shown in the evasion flux rate maps over stream and river areas in April, June and September (Fig. S8a-b). Stream evasion (Fig. S8a), tends to be broadly distributed over the whole basin, representing the fact that small streams and their evasion are the main hydrologic connectors outside of the main river and tributary grid cells, whereas river evasion (Fig. S8b) is clearly linked to the hydrographic representation of the Lena main stem itself, with higher total quantities in some individual grid cells than for the stream reservoir, yet distributed amongst a substantially smaller number of grid cells. Whereas the stream reservoir has greatest absolute evasion flux rates earlier in the year (April-May), maximum evasion rates occur later in the year and further downstream for the river reservoir, reflecting the fact that headwaters are first-order integrators of soil-water carbon connectivity, whereas the river mainstem and tributaries are of a secondary order.

The spatio-temporal pattern of increasing evasion over the simulation period is shown in Fig. S7 as a Hovmöller difference plot, between the last and first decade, of log-scale average monthly evasion rates per latitudinal band. This shows that the vast majority of outgassing increase occurs between March and June, corresponding to the progressive onset of the thaw period moving northwards over this timespan. Although relatively small, outgassing increases are apparent for most of the year, particularly at lower latitudes. This would suggest that the change is driven most acutely by relatively greater temperature increases at higher latitudes ('Arctic amplification' of climate warming, e.g. Bekryaev et al., 2010) while less acute but more temporally homogenous evasion is driven by seasonal warming at lower latitudes.

Text S8:

This is because in ORCHIDEE MICT-L, the 'stream' water reservoir is water routed to the river network for all hydrologic flows calculated to not cross a 0.5 degree grid cell boundary (the resolution of the routing module, explained in Part 1, Section 2.6), which may not be commensurate with long, <20m width streams in the real-world, that were used in the Denfeld et al. (2013) study. In addition, this 'stream' water reservoir in the model does not include any values for width or area in the model, so we cannot directly compare our stream reservoir to the <20m width criterion employed by Denfeld et al. (2013) in their definition of an observed stream. Thus our 'stream' water reservoir encompasses substantially greater surface area and hydrologic throughput than that in the Denfeld et al. study.

Text S9:

The 'approximate' caveat refers to the fact that model output doesn't define a precise surface area for the stream water reservoir, which is instead bundled into a single value representing the riverine fraction of a grid cell's total surface area. To approximate the areal outgassing for the stream versus river water reservoirs, we weight the total non-floodplain inundated area of each grid cell by the relative total water mass of each of the two hydrological pools, then divide the total daily CO_2 flux simulated by the model by this value. The per-pool areal estimate is an approximation since it assumes that rivers and streams have the same surface area: volume relationship. This is clearly not the case, since streams are generally shallow, tending to have greater surface area per increment increase in depth than rivers. Thus, our areal approximations are likely underestimated (overestimated) for streams (rivers), respectively. Note that from ~700 non-zero simulation datapoints used to generate Fig. 6d were omitted as 'outliers' from the stream reservoir efflux statistics described below, because very low stream:river reservoir values skewed the estimation of total approximate stream surface area values very low, leading to extreme efflux rate values of 1-3000gC m^{-2} d^{-1} and are thus considered numerical artefacts of the areal approximation approach used here.

Text S10: Emergent Phenomena: DOC and Topographic Slope

This relationship was found in temperate rivers by Lauerwald et al. (2012), and in a recent Pan-Arctic synthesis paper Connolly et al. (2018). The reasoning for the negative slope-DOC concentration relationship is that as elevation increases, temperature and primary production decreases. This leads to a thinner organic soil layer, meaning that mineral soil plays a stronger role in shallow hydrologic flowpaths, allowing for deeper infiltration and shorter residence time in a given soil layer. Further, steeper terrain leads to a lower soil water residence time and lower moisture than in flat areas. As a result, a given patch of soil matter will be exposed to leaching for less (residence) time, while the organic matter that is leached is thought to be adsorbed more readily to mineral soil particles, leading to either their re-stabilisation in the soil column or shallow retention and subsequent heterotrophic respiration in situ, cumulatively resulting in lower DOC concentrations in the hydrologic export (Kaiser and Kalbitz, 2012; Klaminder et al., 2011). This line of reasoning was recently shown to apply also to deep organic permafrost soils (Zhang et al., 2017), although the degree to which this is the case in comparison to mineral soils is as yet unknown.

In addition, and as described in Part 1 (Section 2.5) of this study, MICT-L contains a provision for increased soil column infiltration and lower decomposition rates in areas underlain by Podzols and Arenosols. The map from the Harmonized World Soil Database (Nachtergaele, Freddy, Harrij van Velthuizen, Luc Verelst, N. H. Batjes, Koos Dijkshoorn, V. W. P. van Engelen, Guenther Fischer, Arwyn Jones, Luca Montanarella, Monica Petri, Sylvia PrielerB, Xuezheng Shi, Edmar Teixera and David Wiberg, 2010), which is used as the input to this criterion, shows areas underlain by these soils in the Lena basin to also be co-incident with areas of high topographic slope (Fig. 3a, SI, Fig S9b). The 'Podzol effect' is to increase the rate of decomposition and infiltration of DOC, relative to all other soil types, thus also increasing the rate of DOC flux into groundwater (see Part 1 of this study, Section 2.5). Thus, our modelling framework explicitly resolves the processes involved in these documented dynamics –soil thermodynamics, solid vertical flow (turbation), infiltration as a function of soil textures and types, adsorption as a function of soil parameters (see Part 1 of this study, Section 2.11), DOC respiration as a function of soil temperature and hence depth (Part 1, Section 2.12), and lagging of DOC vertical flow behind hydrological drainage flow (summary Figure in Part 1, Fig. 1). We thus have some confidence in reporting that the simulated negative relationship of DOC concentration with topographic slope may indeed emerge from the model.

Text S11: Emergent Phenomena: DOC and Mean Annual Air Temperature

A key emergent property of DOC concentrations in soils and inland waters should be their positive partial determination by the temperature of the environment under which their rates of production occur, as has been shown in the literature on permafrost regions, most notably in Frey & Smith (2005) and Frey & McClelland (2009). Increasing temperatures should lead to greater primary production, thaw, decomposition and microbial mobilisation rates, and hence DOC production rates, leading to (dilution effects notwithstanding) higher concentrations of DOC in thaw and so stream waters. Looking at this emergent property allows us to evaluate the soil-level production of both DOC and thaw water at the appropriate biogeographic and temporal scale in our model.

This provides a further constraint on model effectiveness at simulating existing phenomena at greater process-resolution.

Figure 7 compares three datasets (simulated and two observational) of riverine DOC concentration (in mgC L^{-1}) plotted against mean annual air temperature (MAAT). The simulated grid-scale DOC versus MAAT averaged over July and August (for comparability of DOC with observational sampling period) of 1998-2007 is shown in red, and observed data compiled by Laudon et al. (2012) and Frey and Smith (2005) for sites in temperate/cold regions globally and peatland-dominated Western Siberia, respectively. The Laudon et al. (2012) data are taken from 49 observations including MAAT over the period 1997-2011 from catchments north of 43°N, and aggregated to 10 regional biogeographies, along with datapoints from their own sampling; those in the Frey and Smith study are from 55-68°N and ~65-85°E (for site locations, see Laudon et al. (2012), Table 1 and 2; Frey and Smith (2005), Fig. 1).

Fig. 7 can be interpreted in a number of ways. First, this MAAT continuum spans the range of areas that are both highly and moderately permafrost affected and permafrost free (Fig. 7, blue and green versus orange shading, respectively), potentially allowing us a glimpse of the behaviour of DOC concentration as the environment transitions from the former to the latter. Simulated Lena DOC concentrations, all in pixels with MAAT < -2°C and hence all bearing continuous or discontinuous permafrost ('permafrost-affected' in the figure), only exhibit a weakly positive response to MAAT on the scale used ($y=6.05e^{0.03\mathrm{MAAT}}$), although the consistent increase in DOC minima with MAAT is clearly visible. Second, the Laudon et al. (2012) data exhibit an increasing then decreasing trend over the range of MAAT (-2°C to 10°C) in their dataset, which they propose reflects an 'optimal' MAAT range (0-3°C) for the production and transport of DOC (Fig. 7, red shading). Below this optimum range, DOC concentrations may be limited by transport due to freezing, and above this, smaller soil carbon pools and temperature-driven decomposition would suppress the amount of DOC within rivers. Third, the lower end of the Laudon et al. (2012) MAAT values correspond to a DOC concentration in line with DOC concentrations simulated by our model. Fourth, DOC concentrations in the Frey and Smith (2005) data exhibit a broad scattering in permafrost-affected sites, with concentrations overlapping those of our simulations (Fig. 7, green shading), before rapidly increasing to very high concentrations relative to the Laudon et al. (2012) data, as sites transition to permafrost-free (red shading, $y=3.6_{\mathrm{MAAT}}+29.4$).

Their data highlight the difference in DOC concentration regime between areas of high (Frey and Smith, 2005) and low (Laudon et al., 2012) peatland coverage and the different response of these to temperature changes. Fifth, because our simulation results largely correspond with the observed data where the MAAT ranges overlap (green shading), and because our model lacks peatland processes, we should expect our model to follow the polynomial regression plotted for the Laudon et al. (2012) data as temperature inputs to the model increase. Figure 7 implies that this increase should be on the order of a doubling of DOC concentration as a system evolves from a MAAT of -2°C to 2°C. With warming, we expect the response of DOC concentrations to reflect a mix of both observationally-derived curves, as a function of peatland coverage.

Text S12: LOAC drivers

The constant climate (CLIM) and constant CO_2 (CO2) simulations described in Section 3 were undertaken to assess the extent –and the extent of the difference –to which these two factors are drivers of model processes and fluxes. These differences are summarised in Figs. S10 (a-b), in which we show the same 1998-2007 –averaged yearly variable fluxes as in the CTRL simulation, expressed as percentages of the CTRL values given in Fig. 2. A number of conclusions can be drawn from these diagrams.

First, all fluxes are lower in the factorial simulations, which can be expected due to lower carbon input to vegetation from the atmosphere (constant CO_2) and colder temperatures (constant climate) inhibiting more vigorous growth and carbon cycling. Second, broadly speaking, both climate and CO_2 appear to have similar effects on all fluxes, at least within the range of climatic and CO_2 values to which they have subjected the model in these historical runs. With regard to lateral export fluxes in isolation, variable climate (temperature increase) is a more powerful driver than CO_2 increase (see below). Third, the greatest difference between the constant climate and CO_2 simulation carbon fluxes appear to be those associated with terrestrial inflow of dissolved matter to the aquatic network, these being more sensitive to climatic than CO_2 variability. This is evidenced by a 49% and 32% decline in CO_2 and DOC export, respectively, from the land to rivers in the constant climate simulation, versus a 27% and 23% decline in these same variables in the constant CO_2 simulation. Given that the decline in primary production and respiration in both factorial simulations was roughly the same, this difference in terrestrial dissolved input is attributable to the effect of climate (increased temperatures) on the hydrological cycle, driving changes in lateral export fluxes.

This would imply that at these carbon dioxide and climatic ranges, the modelled DOC inputs are slightly more sensitive to changes in the climate rather than to changes in atmospheric carbon dioxide concentration and the first order biospheric response to this. However, while the model biospheric response to carbon dioxide concentration may be linear, thresholds in environmental variables such as MAAT may prove to be tipping points in the system's emergent response to change, as implied by Fig. 7, meaning that the Lena, as with the Arctic in general, may soon become much more temperature-dominated with regard to the drivers of its own change.

Supplementary Tables and Figures

Table S1: Data type, name and sources of data files used to drive the model in the study simulations.

Data Type	Name	Source
Vegetation Map	ESA CCI Land Cover Map	(Bontemps et al., 2013)
Topographic Index	STN-30p	(Vorosmarty et al., 2000)
Stream flow direction	STN-30p	Vörösmarty et al., 2000
River surface area		(Lauerwald et al., 2015)
Soil texture class		(Reynolds et al., 1999)
Climatology	GSWP3 v0, 1 degree	http://hydro.iis.u-tokyo.ac.jp/GSWP3/

Potential floodplains	Multi-source global wetland maps	(Tootchi et al., 2019)
Poor soils	Harmonized World Soil Database map	(Nachtergaele, Freddy, Harrij van Velthuizen, Luc Verelst, N. H. Batjes, Koos Dijkshoorn, V. W. P. van Engelen, Guenther Fischer, Arwyn Jones, Luca Montanarella, Monica Petri, Sylvia PrielerB, Xuezheng Shi, Edmar Teixera and David Wiberg, 2010)
Spinup Soil Carbon Stock	20ky ORCHIDEE-MICT soil carbon spinup	(Guimberteau et al., 2018)

Table S2: Literature sources for empirical evaluation of model output.

	Empirical Evaluation Sources
DOC Discharge	Cauwet and Sidorov (1996); Dolman et al. (2012); Holmes et al. (2012); Lara et al. (1998); Raymond et al. (2007); Semiletov et al. (2011); Kutscher et al. (2017).
Water Discharge	Ye et al. (2009); Lammers et al. (2001)
DOC concentration	Shvartsev (2008); Denfeld et al. (2013); Mann et al. (2015); Raymond et al. (2007); Semiletov et al. (2011); Arctic-GRO/PARTNERS (Holmes et al., 2012)
NPP	Beer et al. (2006); Lloyd et al. (2002); Roser et al. (2002); Schulze et al. (1999); Shvidenko and Nilsson, (2003)
Soil Respiration	Elberling (2007); Sawamoto et al. (2000); Sommerkorn (2008).
CO2 Evasion	Denfeld et al. (2013); Serikova et al. (2018).

Table S3: Observed versus simulated DOC discharge (1998-2007), where we compare the output of two separate climatological datasets used as input to the model (GSWP3 and ISIMIP 2b). Also shown are the simulated versus observed DOC discharge for the six largest Arctic rivers (the "Big Six") and for the Pan-Arctic as a whole.

	Simulated DOC to Ocean	Simulated DOC to Ocean	Observations (Holmes et al., 2012)
	GSWP3	**ISIMIP 2b**	**PARTNERS/Arctic-GRO**
Lena	3.16	4.14	5.68
Big 6		19.36	18.11
Pan-Arctic		32.06	34.04

Table S4: Mean observed groundwater CO_2 and DOC concentrations for global permafrost regions subdivided by biogeographic province and compiled by Shvartsev (2008) from over 9000 observations.

	Permafrost Groundwater Provinces				
	Swamp	Tundra	Taiga	Average	Average (-Swamp)
CO_2 (mgC L^{-1})	12.3	14	10.8	12.4	12.4
DOC (mgC L^{-1})	17.6	10.1	9.3	12.3	9.7

(a)

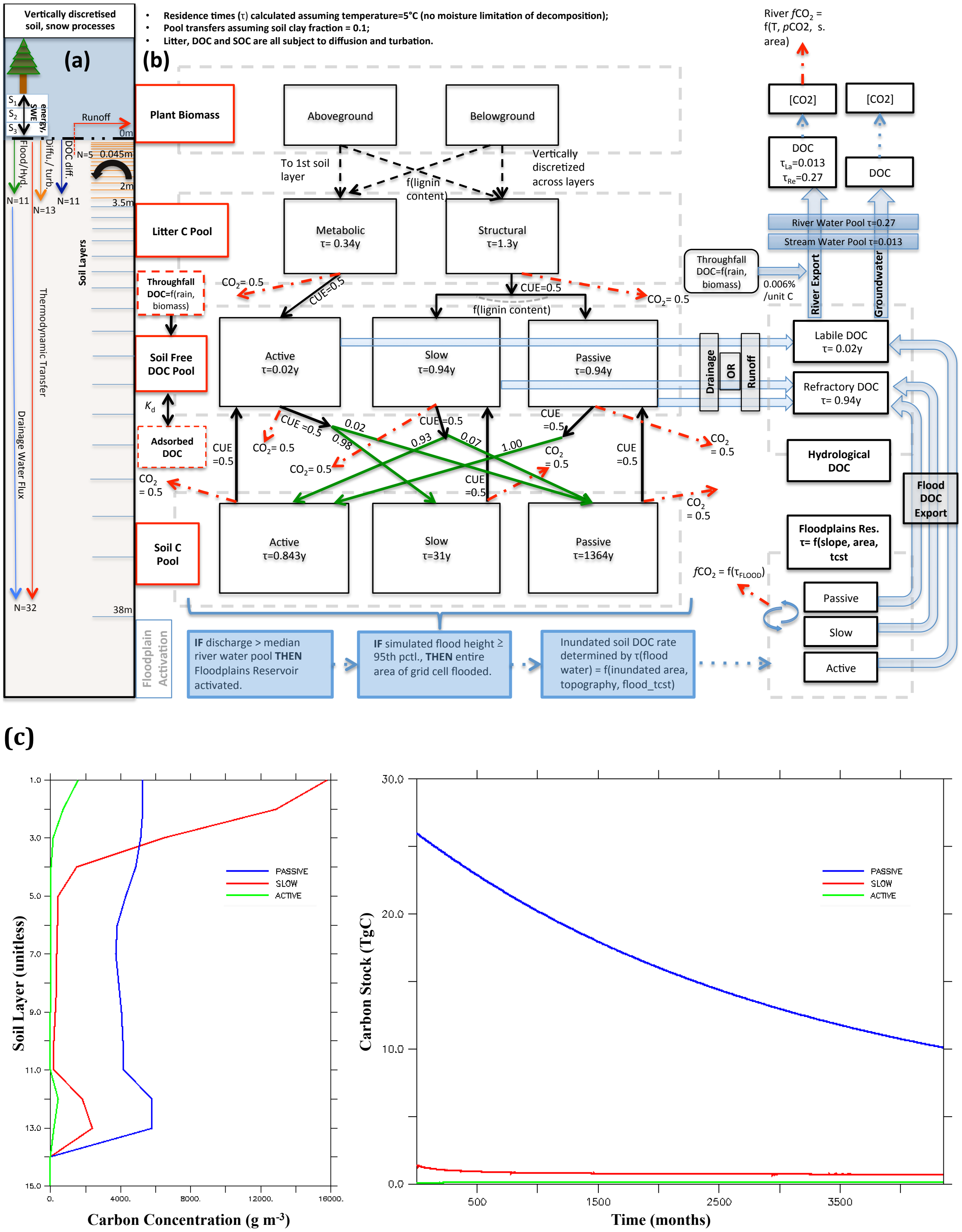

Figure S1: (a-b) Carbon and water flux map for core DOC elements in model structure relating to DOC transport and transformation, first published in Part 1 of this study. **(a)** Summary of the differing extent of vertical discretisation of soil and snow for different processes calculated in the model. Discretisation occurs along 32 layers whose thickness increases geometrically from 0-38m. N refers to the number of layers, SWE=snow water equivalent, S_n = Snow layer n. Orange layers indicate the depth to which diffusive carbon (turbation) fluxes occur. **(b)** Conceptual map of the production, transfer and transformation of carbon in its vertical and lateral (i.e., hydrological) flux as calculated in the model. Red boxes indicate meta-reservoirs of carbon, black boxes the actual pools as they exist in the model. Black arrows indicate carbon fluxes between pools, dashed red arrows give carbon loss as CO_2, green arrows highlight the fractional distribution of DOC to SOC (no carbon loss incurred in this transfer), a feature of this model. For a given temperature (5°C) and soil clay fraction, the fractional fluxes between pools are given for each flux, while residence times for each pool (τ) are in each box. The association of carbon dynamics with the hydrological module are shown by the blue arrows. Blue coloured boxes illustrate the statistical sequence which activates the boolean floodplains module. Note that for readability, the generation and lateral flux of dissolved CO_2 is omitted from this diagram, but is described at length in the Methods section. **(c)** (Left) Soil carbon concentrations per depth level for each soil carbon reactivity pool at the end of the spinup period. (Right) Evolution of each soil carbon pool over the course of the 400-year spinup quasi-eqliuibration period.

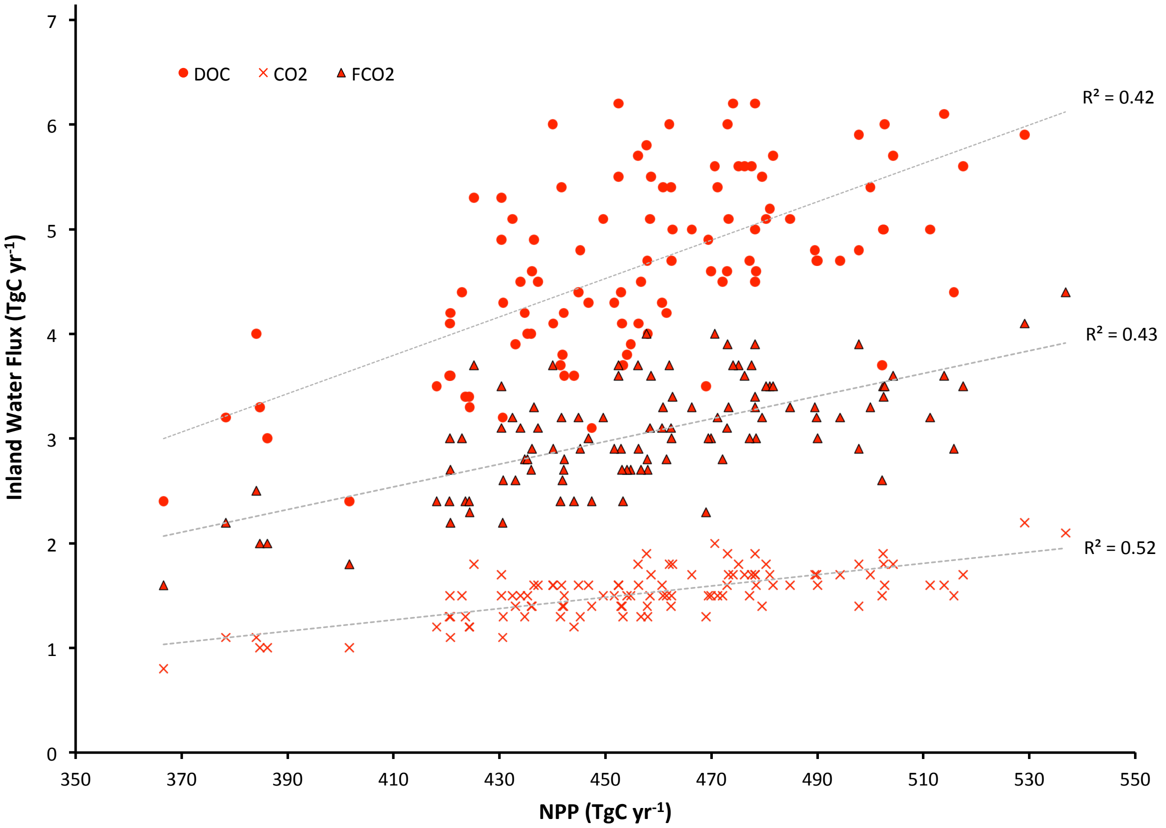

Figure S2: Summed yearly lateral flux versus NPP values for DOC discharge, CO_2 discharge and CO_2 evasion (FCO_2) over the entire simulation period, with linear regression lines shown.

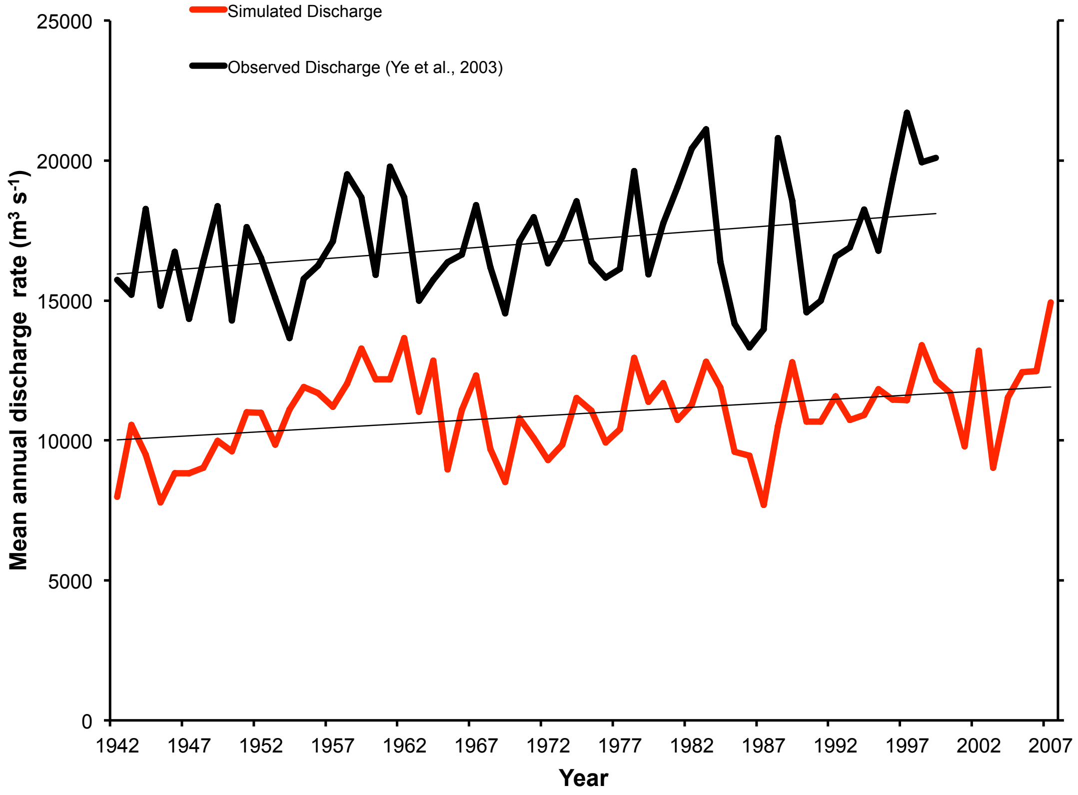

Figure S3: Observed versus simulated mean annual water discharge from the Lena river, where observations are taken from (Ye et al., 2003).

(a)

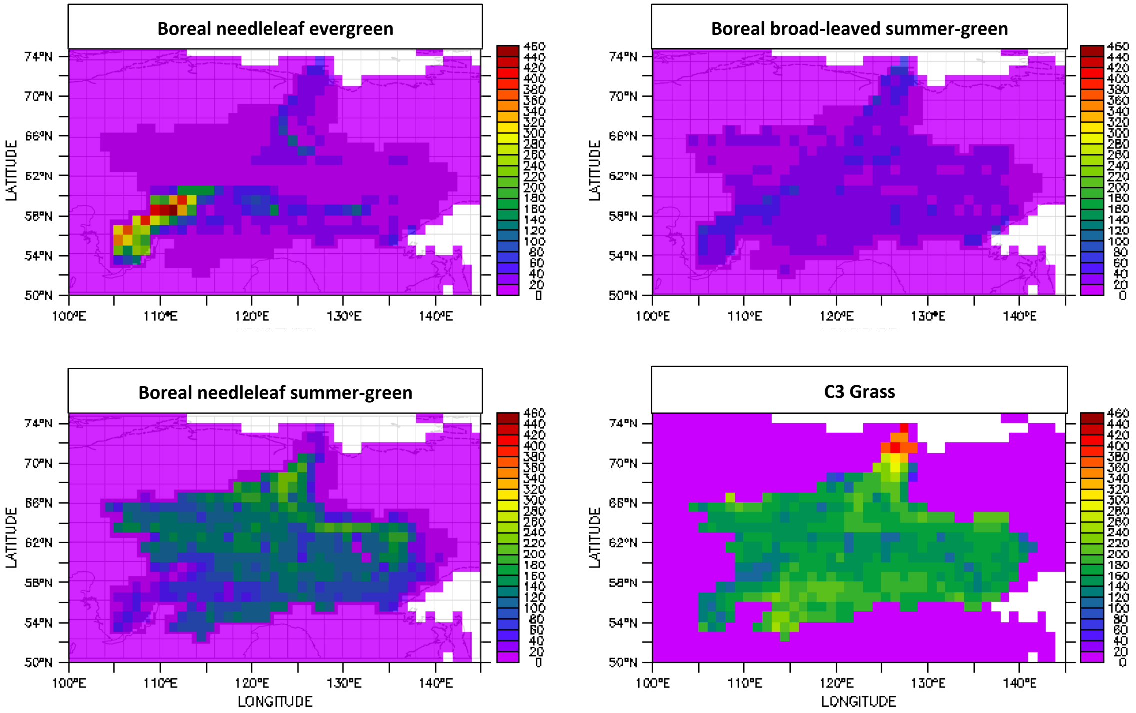

(b)

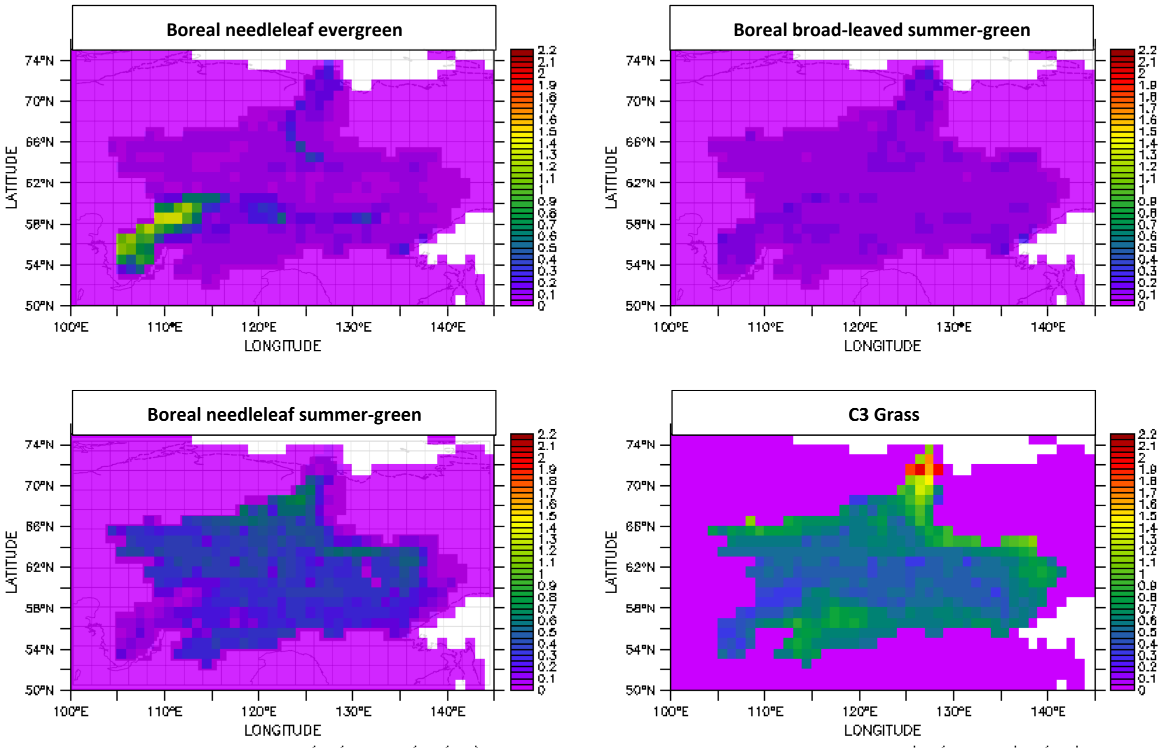
Boreal needleleaf evergreen
Boreal broad-leaved summer-green
Boreal needleleaf summer-green
C3 Grass
74°N
70°N
66°N
62°N
58°N
54°N
50°N
LATITUDE
100°E
110°E
120°E
130°E
140°E
LONGITUDE
2.2
2.1
2
1.9
1.8
1.7
1.6
1.5
1.4
1.3
1.2
1.1
1
0.9
0.8
0.7
0.6
0.5
0.4
0.3
0.2
0.1
0

(c)

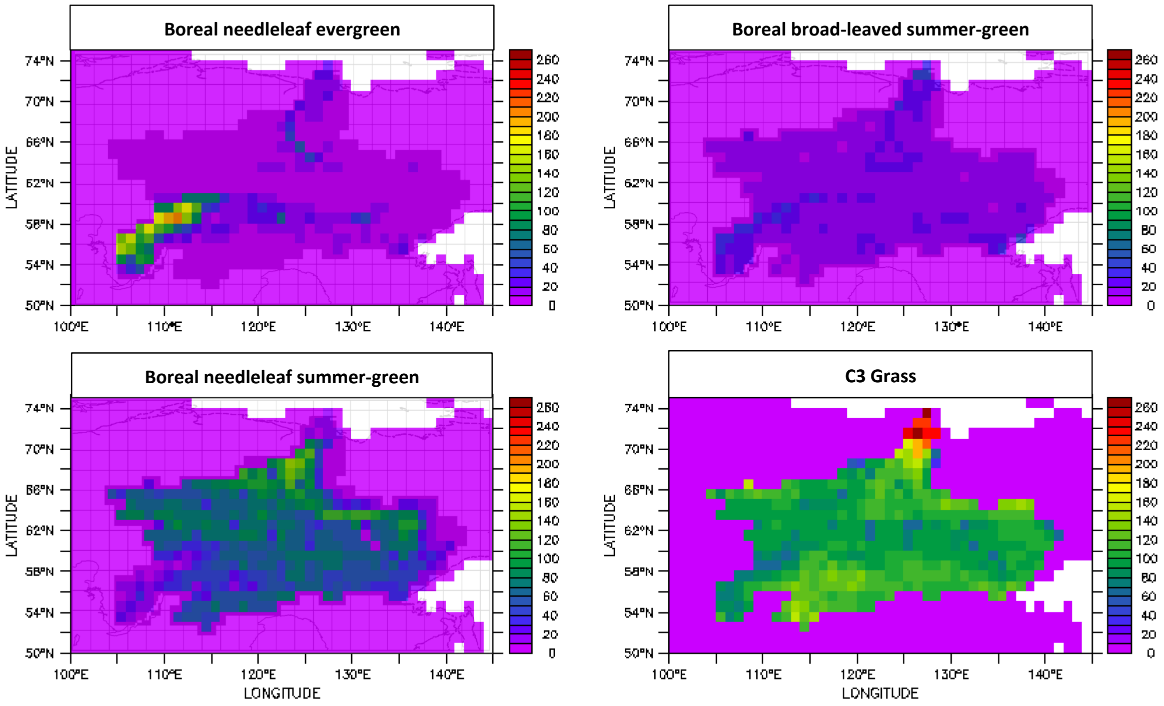
Boreal needleleaf evergreen
Boreal broad-leaved summer-green
Boreal needleleaf summer-green
C3 Grass
74°N
70°N
66°N
62°N
58°N
54°N
50°N
LATITUDE
100°E
110°E
120°E
130°E
140°E
LONGITUDE
260
240
220
200
180
160
140
120
100
80
60
40
20
0

(d)

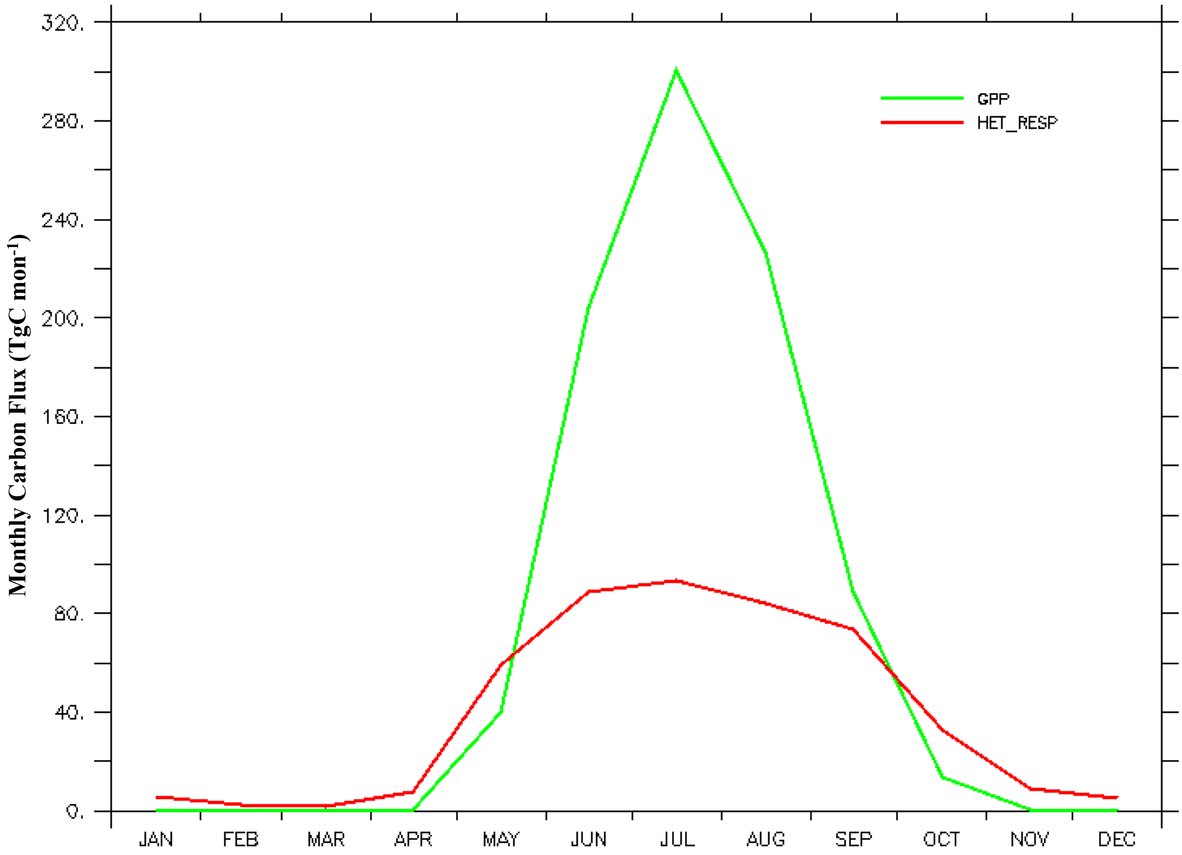

Figure S4: (a) Absolute yearly gross primary productivity (GPP, TgC yr^{-1}) for the four relevant PFT groups over the Lena basin, averaged over 1998-2007. (b) Mean July and August soil heterotrophic respiration rates (g m^2 d^{-1}) for the same PFT groups as in (a), during the period 1998-2007. (c) Average yearly NPP (gC m^2 yr^{-1}) averaged over the period 1998-2007. All maps have the Lena basin area shaded in the background. (d) Mean monthly carbon uptake (GPP) versus its heterotrophic respiration from the soil (Het_Resp) in TgC per month, over the period 1998-2007.

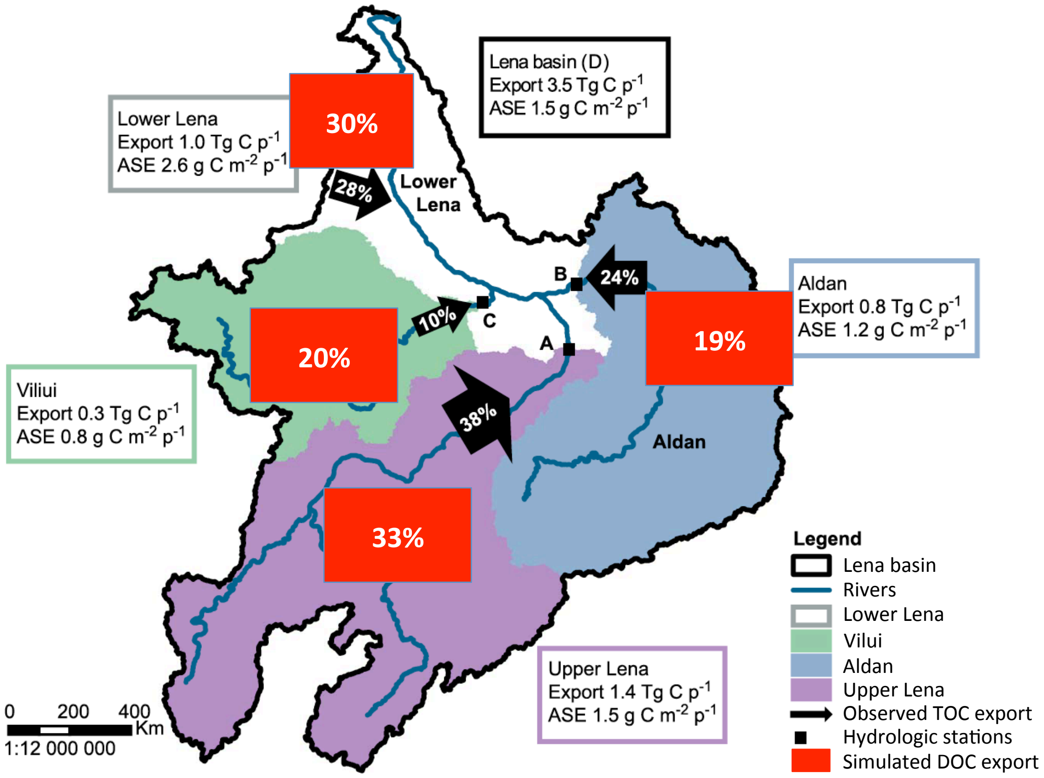

Figure S5: Map adapted from Fig. 2 in Kutscher et al. (2017) showing proportional sub-basin contributions of TOC outflow to total TOC discharge in June and July (designated as their sampling period 'p^{-1}') of 2012-2013, as observed in Kutscher et al., 2017 (black arrows), and DOC export contributions as simulated over the period 1998-2007 by ORCHIDEE MICT-L (red boxes). Simulation pixels used in the calculation are correlates of the real-world sampling locations unless the site coordinates deviated from a mainstem hydrographic flowpath pixel –in which case a nearest ‘next-best’ pixel was used. Here the percentages are out of the summed mean bulk DOC flow of each tributary, not the mean DOC discharge from the river mouth, because doing so would negate the in-stream loss of DOC via degradation to CO_2 while in-stream.

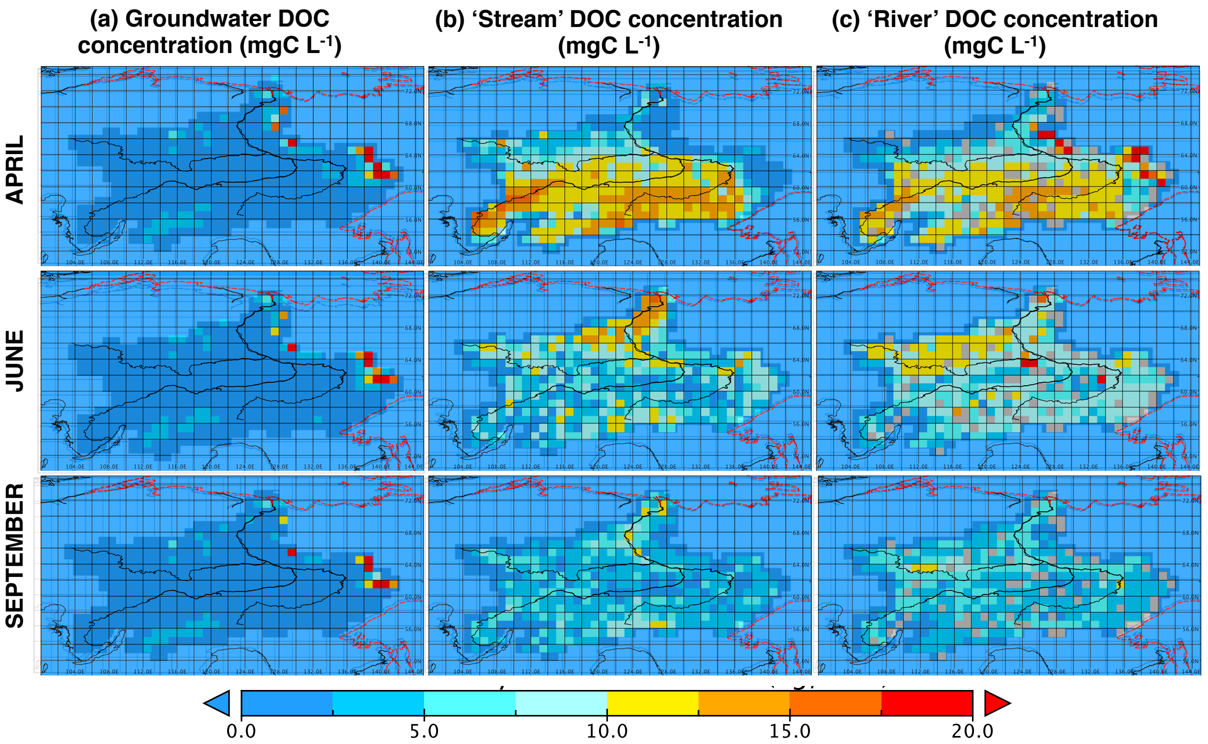

Figure S6: Maps of **(a)** DOC concentrations (mgC L^{-1}) in groundwater ('slow' water pool), **(b)** stream water pool, **(c)** river water pool in April, June and September (first to third rows, respectively), averaged over the period 1998-2007. The coastal boundary and a water body overlay have been applied to the graphic in red and black, respectively, and the same scale applies to all diagrams. All maps have the Lena basin area shaded in the background.

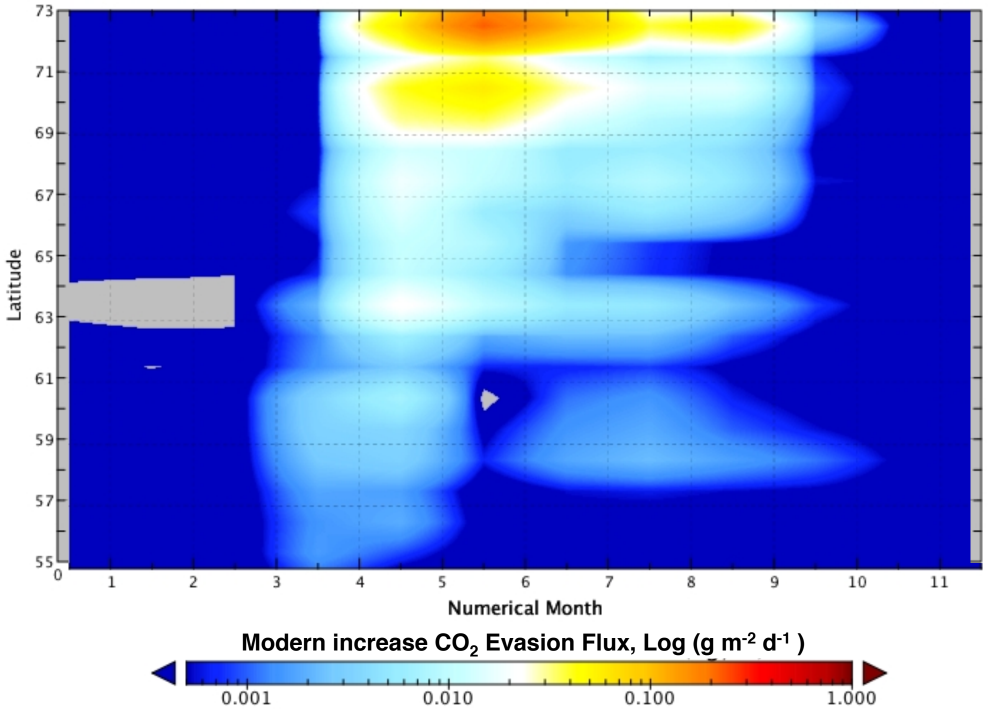

Figure S7: Log-scale Hovmöller diagram plotting the longitudinally-averaged difference (increase) in total CO$_2$ evaded from the Lena River basin between the average of the periods 1998-2007 and 1901-1910, over each montly timestep, in (log) gC m^{-2} d^{-1}. Thus as the river drains northward the month-on-month difference in water-body CO_2 flux, between the beginning and end of the 20th Century is shown.

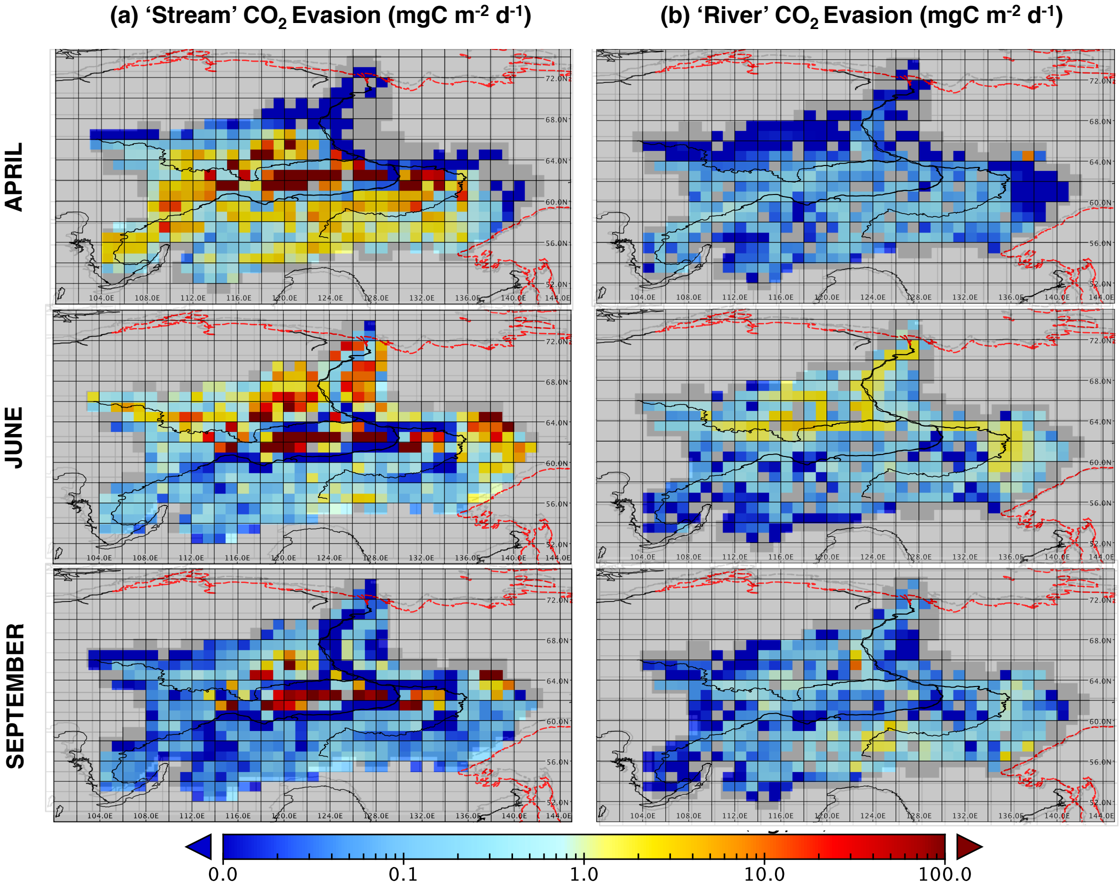

Figure S8: Maps of CO_2 evasion from the surface of the two fluvial hydrological pools in the model, (a) streams and (b) rivers in April, June and September. All maps use the same (log) scale in units of (mgC m^{-2} d^{-1}).

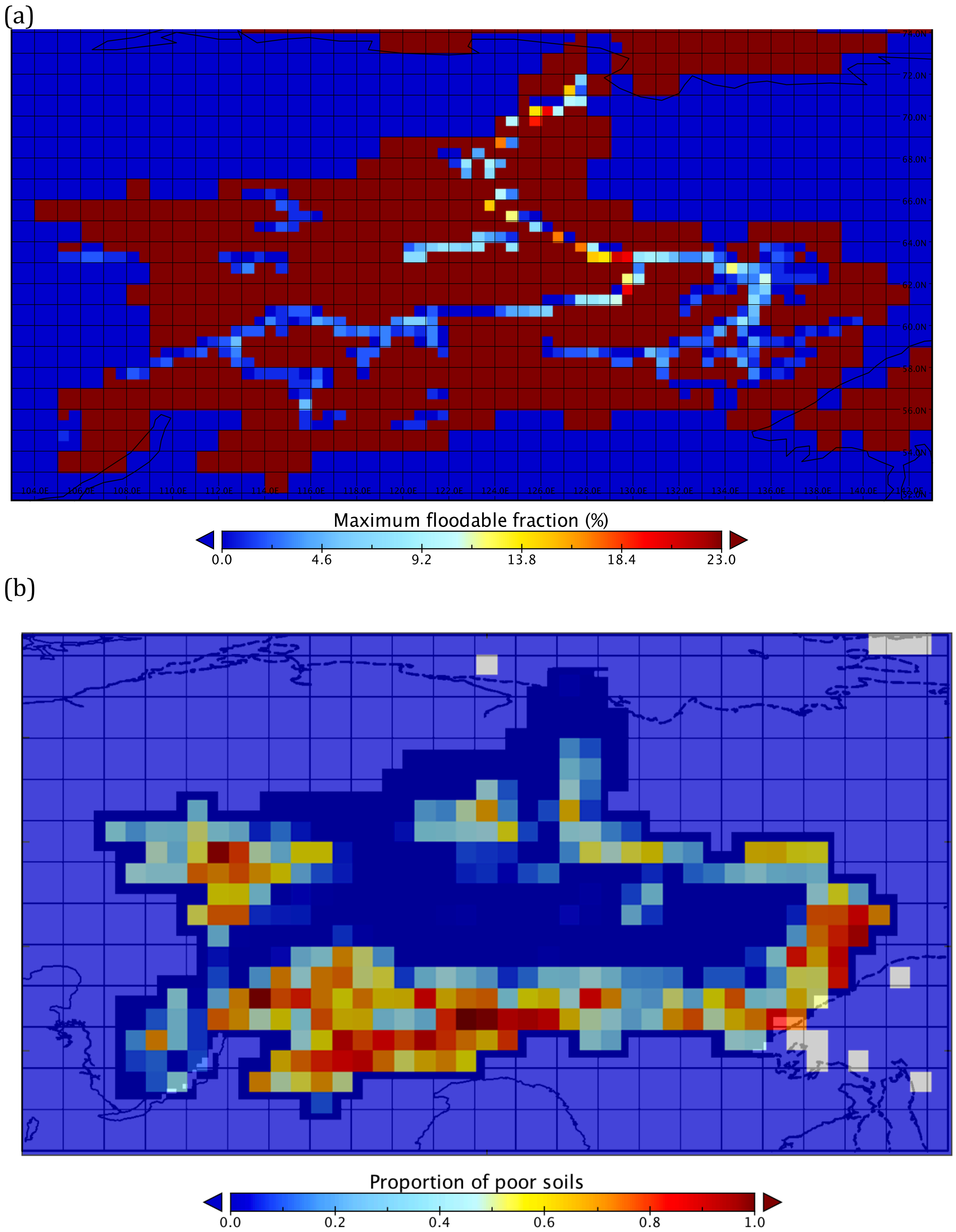

Figure S9: (a) Maximum floodable fraction of grid cells for the Lena basin per the input map from Tootchi et al. (2018). (b) Podzol and Arenosol map (Nachtergaele, Freddy, Harrij van Velthuizen, Luc Verelst, N. H. Batjes, Koos Dijkshoorn, V. W. P. van Engelen, Guenther Fischer, Arwyn Jones, Luca Montanarella, Monica Petri, Sylvia PrielerB, Xuezheng Shi, Edmar Teixera and David Wiberg, 2010) used as input to the ‘poor soils’ module, basin mask in the background.

(a)

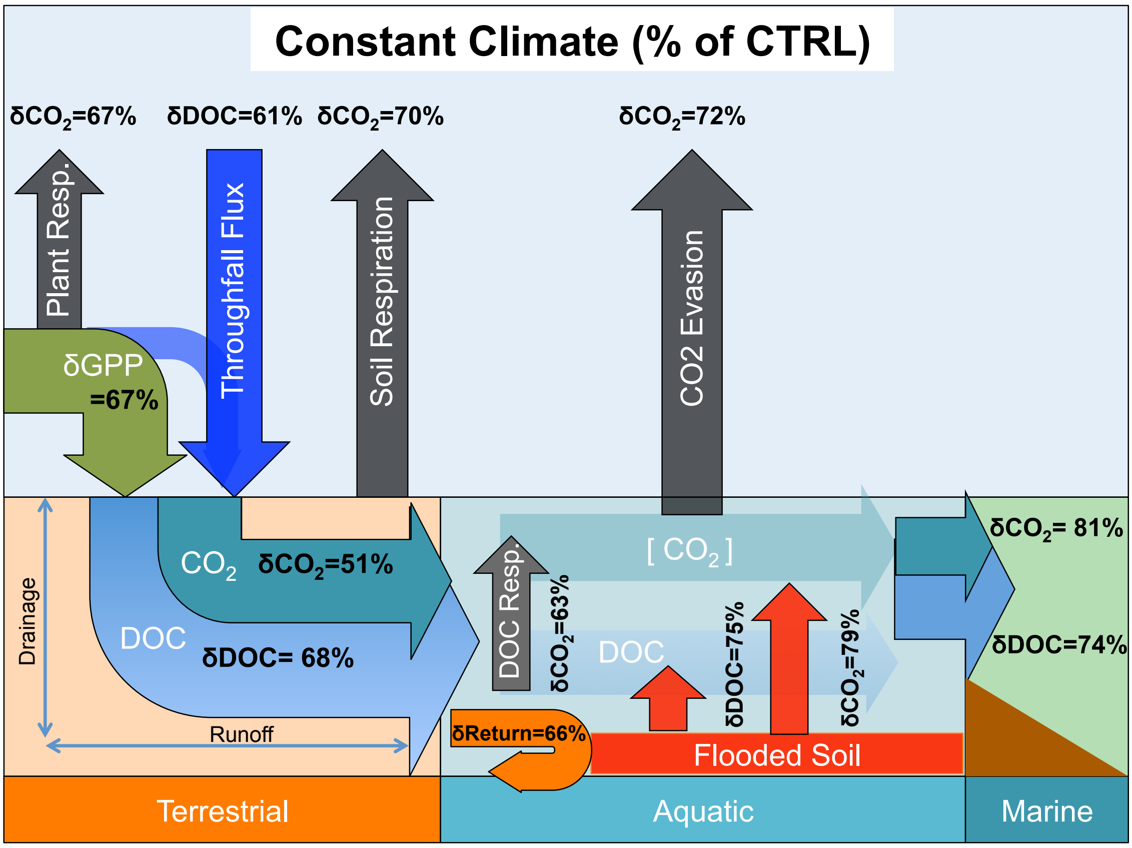
Constant Climate (% of CTRL)
δCO$_2$=67%
δDOC=61%
δCO$_2$=70%
δCO$_2$=72%
Plant Resp.
Throughfall Flux
Soil Respiration
CO2 Evasion
δGPP
=67%
CO$_2$
δCO$_2$=51%
DOC
δDOC= 68%
Drainage
Runoff
DOC Resp.
δCO$_2$=63%
[CO$_2$]
DOC
δDOC=75%
δCO$_2$=79%
δReturn=66%
Flooded Soil
δCO$_2$= 81%
δDOC=74%
Terrestrial
Aquatic
Marine

(b)

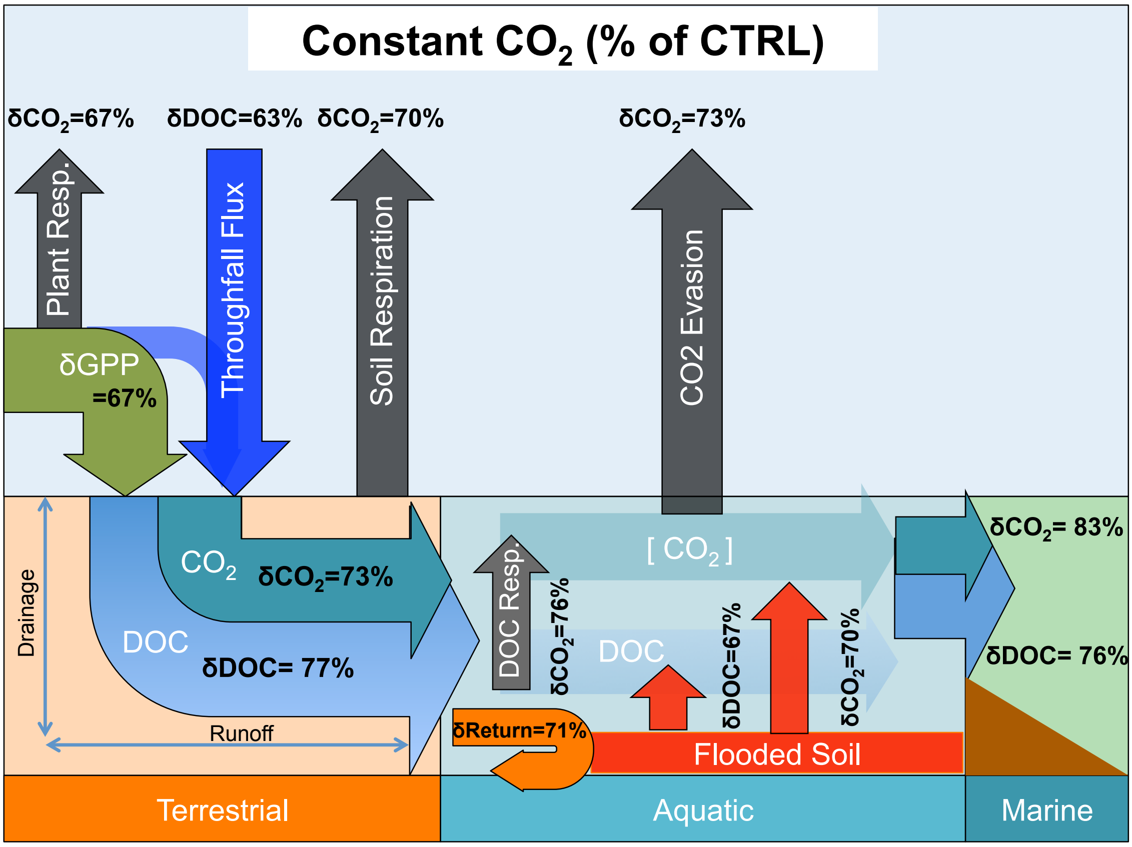
Constant CO$_2$ (% of CTRL)
δCO$_2$=67%
δDOC=63%
δCO$_2$=70%
δCO$_2$=73%
Plant Resp.
Throughfall Flux
Soil Respiration
CO2 Evasion
δGPP
=67%
CO$_2$
δCO$_2$=73%
DOC
δDOC= 77%
Drainage
Runoff
DOC Resp.
δCO$_2$=76%
[CO$_2$]
DOC
δDOC=67%
δCO$_2$=70%
δReturn=71%
Flooded Soil
δCO$_2$= 83%
δDOC= 76%
Terrestrial
Aquatic
Marine

Figure S10: (a-b): Schematic diagrams detailing the major yearly carbon flux outputs from simulations averaged over the period 1998-2007 as they are transformed and transported across the land-aquatic continuum. Figures **(b)** and **(c)** give the same fluxes as a percentage difference from the Control (CTRL-Simulation), for the constant climate and CO_2 simulations, respectively.

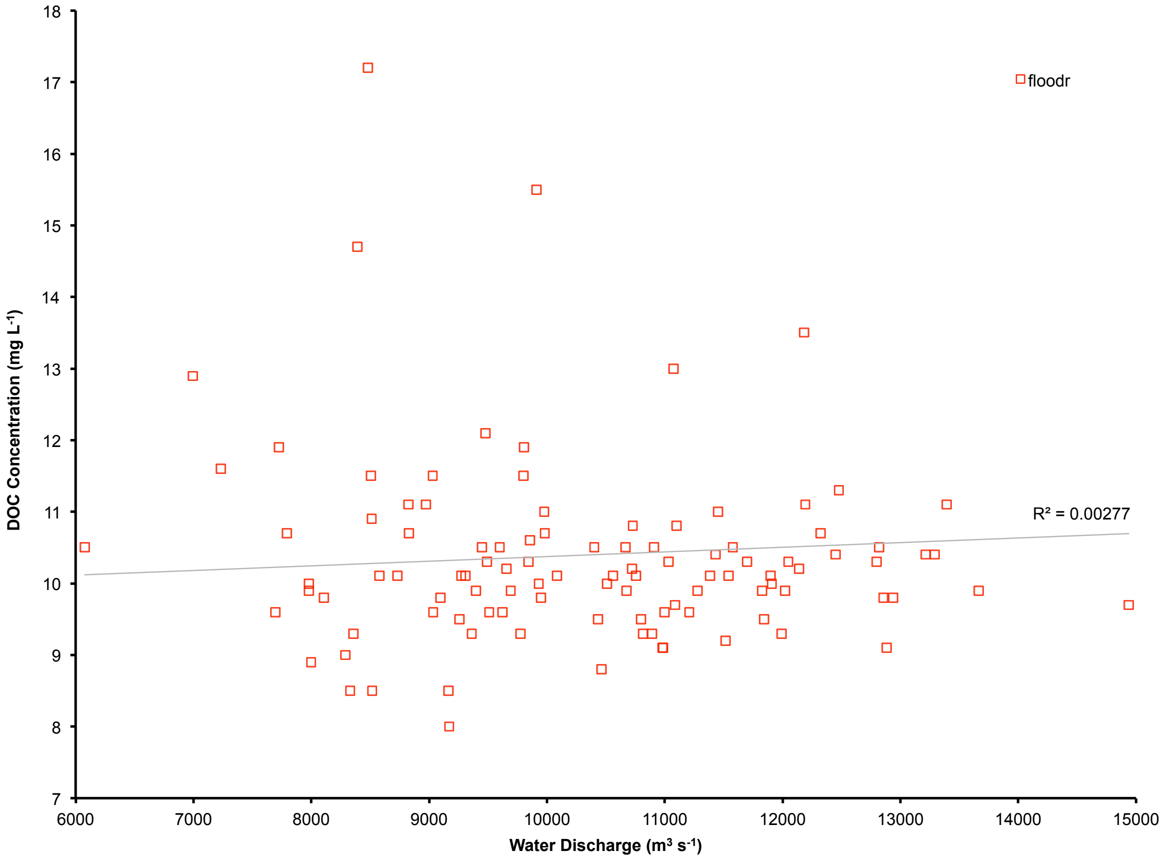

Figure S11: Simulated basin-mean annual DOC concentrations (mg L^{-1}) for the floodplain water pool regressed against mean annual simulated discharge rates at Kusur (m^3 s^{-1}) over 1901-2007. A linear regression with R^2 is plotted.

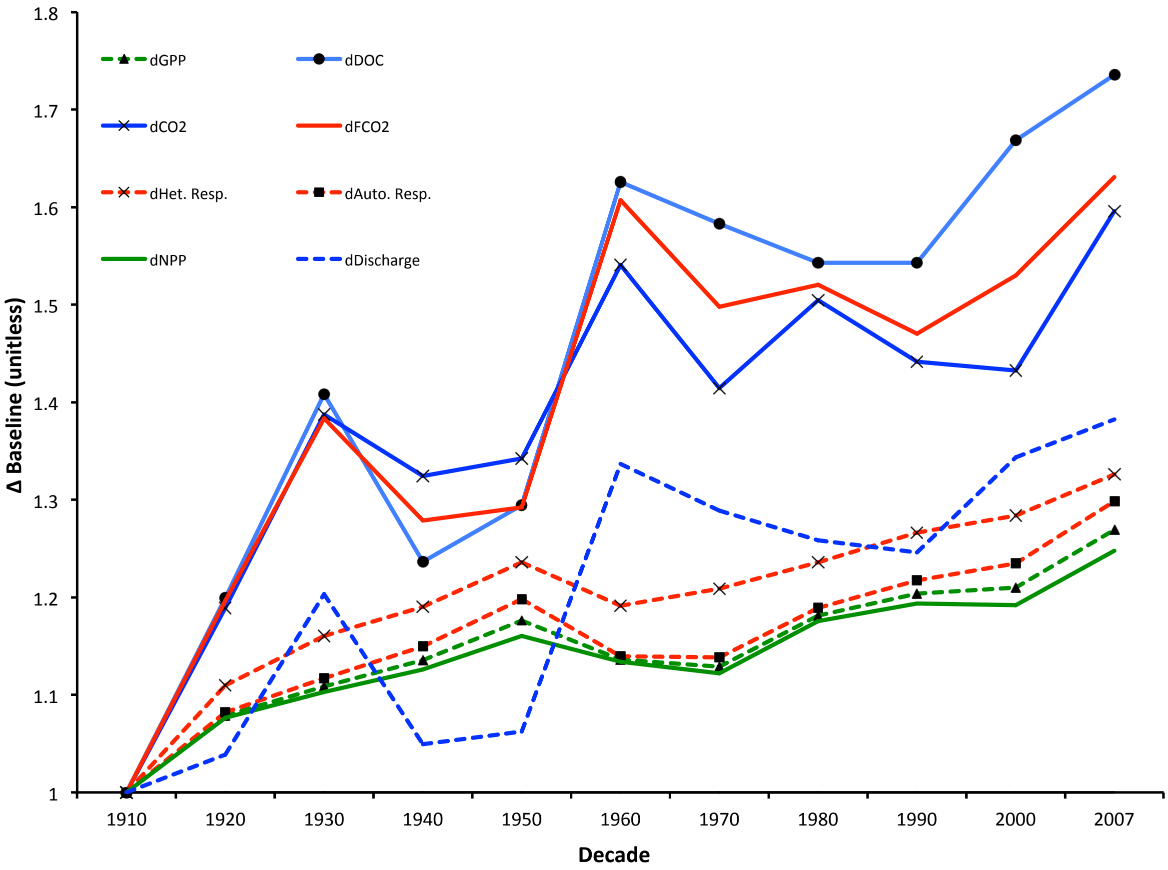

Figure S12: Time series showing the decadal-mean fractional change in carbon fluxes normalised to a 1901-1910 average baseline (=1 on the y-axis) for NPP, GPP, autotrophic and heterotrophic respiration, DOC inputs to the water column, CO_2 inputs to the water column, CO_2 evasion from the water surface (FCO2), and discharge.

References

Beer, C., Lucht, W., Schmullius, C. and Shvidenko, A.: Small net carbon dioxide uptake by Russian forests during 1981-1999, Geophys. Res. Lett., doi:10.1029/2006GL026919, 2006.

Bekryaev, R. V., Polyakov, I. V. and Alexeev, V. A.: Role of polar amplification in long-term surface air temperature variations and modern arctic warming, J. Clim., doi:10.1175/2010JCLI3297.1, 2010.

Biancamaria, S., Bates, P. D., Boone, A. and Mognard, N. M.: Large-scale coupled hydrologic and hydraulic modelling of the Ob river in Siberia, J. Hydrol., doi:10.1016/j.jhydrol.2009.09.054, 2009.

Bontemps, S., Defourny, P., Radoux, J., Van Bogaert, E., Lamarche, C., Achard, F., Mayaux, P., Boettcher, M., Brockmann, C., Kirches, G., Zülkhe, M., Kalogirou, V., Seifert, F. . and Arino, O.: Consistent global land cover maps for climate modelling communities: current achievements of the ESA' and cover CCI, in ESA Living Planet Symposium 2013, pp. 9–13., 2013.

Burke, E. J., Dankers, R., Jones, C. D. and Wiltshire, A. J.: A retrospective analysis of pan Arctic permafrost using the JULES land surface model, Clim. Dyn., doi:10.1007/s00382-012-1648-x, 2013.

Connolly, C. T., Khosh, M. S., Burkart, G. A., Douglas, T. A., Holmes, R. M., Jacobson, A. D., Tank, S. E. and McClelland, J. W.: Watershed slope as a predictor of fluvial dissolved organic matter and nitrate concentrations across geographical space and catchment size in the Arctic, Environ. Res. Lett., 13(10), 104015, doi:10.1088/1748-9326/aae35d, 2018.

Denfeld, B., Frey, K. and Sobczak, W.: Summer CO 2 evasion from streams and rivers in the Kolyma River basin, north-east Siberia, Polar Res., 32(1), 19704, doi:10.3402/polar.v32i0.19704, 2013.

Drake, T. W., Wickland, K. P., Spencer, R. G. M., McKnight, D. M. and Striegl, R. G.: Ancient low–molecular-weight organic acids in permafrost fuel rapid carbon dioxide production upon thaw, Proc. Natl. Acad. Sci., 112(45), 13946–13951, doi:10.1073/pnas.1511705112, 2015.

Elberling, B.: Annual soil CO2effluxes in the High Arctic: The role of snow thickness and vegetation type, Soil Biol. Biochem., doi:10.1016/j.soilbio.2006.09.017, 2007.

Fekete, B. M., Vörösmarty, C. J., Roads, J. O. and Willmott, C. J.: Uncertainties in precipitation and their impacts on runoff estimates, J. Clim., doi:10.1175/1520-0442(2004)017<0294:UIPATI>2.0.CO;2, 2004.

Frey, K. E. and McClelland, J. W.: Impacts of permafrost degradation on arctic river biogeochemistry, Hydrol. Process., 169–182, doi:10.1002/hyp.7196, 2009.

Frey, K. E. and Smith, L. C.: Amplified carbon release from vast West Siberian peatlands by 2100, Geophys. Res. Lett., doi:10.1029/2004GL022025, 2005.

Frieler, K., Lange, S., Piontek, F., Reyer, C. P. O., Schewe, J., Warszawski, L., Zhao, F., Chini, L., Denvil, S., Emanuel, K., Geiger, T., Halladay, K., Hurtt, G., Mengel, M., Murakami, D., Ostberg, S., Popp, A., Riva, R., Stevanovic, M., SuzGBRi, T., Volkholz, J., Burke, E., Ciais, P., Ebi, K., Eddy, T. D., Elliott, J., Galbraith, E., Gosling, S. N., Hattermann, F., Hickler, T., Hinkel, J., Hof, C., Huber, V., Jägermeyr, J., Krysanova, V., Marcé, R., Müller Schmied, H., Mouratiadou, I., Pierson, D., Tittensor, D. P., Vautard, R., Van Vliet, M., Biber, M. F., Betts, R. A., Leon Bodirsky, B., Deryng, D., Frolking, S., Jones, C. D., Lotze, H. K., Lotze-Campen, H., Sahajpal, R., Thonicke, K., Tian, H. and Yamagata, Y.: Assessing the impacts of 1.5ĝ€°C global warming - Simulation protocol of the Inter-Sectoral Impact Model Intercomparison Project (ISIMIP2b), Geosci. Model Dev., doi:10.5194/gmd-10-4321-2017, 2017.

Guimberteau, M., Zhu, D., Maignan, F., Huang, Y., Yue, C., Dantec-N d lec, S., Ottl, C., Jornet-Puig, A., Bastos, A., Laurent, P., Goll, D., Bowring, S., Chang, J., Guenet, B., Tifafi, M., Peng, S., Krinner, G., Ducharne, A. s., Wang, F., Wang, T., Wang, X., Wang, Y., Yin, Z., Lauerwald, R., Joetzjer, E., Qiu, C., Kim, H. and Ciais, P.: ORCHIDEE-MICT (v8.4.1), a land surface model for the high latitudes: model description and validation, Geosci. Model Dev., 11(1), 121–163, doi:10.5194/gmd-11-121-2018, 2018.

Haddeland, I., Clark, D. B., Franssen, W., Ludwig, F., Voß, F., Arnell, N. W., Bertrand, N., Best, M., Folwell, S., Gerten, D., Gomes, S., Gosling, S. N., Hagemann, S., Hanasaki, N., Harding, R., Heinke, J., Kabat, P., Koirala, S., Oki, T., Polcher, J., Stacke, T., Viterbo, P., Weedon, G. P. and Yeh, P.: Multimodel Estimate of the Global Terrestrial Water Balance: Setup and First Results, J. Hydrometeorol., doi:10.1175/2011JHM1324.1, 2011.

Kaiser, K. and Kalbitz, K.: Cycling downwards - dissolved organic matter in soils, Soil Biol. Biochem., doi:10.1016/j.soilbio.2012.04.002, 2012.

Klaminder, J., Grip, H., Mörth, C. M. and Laudon, H.: Carbon mineralization and pyrite oxidation in groundwater: Importance for silicate weathering in boreal forest soils and stream base-flow chemistry, Appl. Geochemistry, doi:10.1016/j.apgeochem.2010.12.005, 2011.

Kutscher, L., Mörth, C. M., Porcelli, D., Hirst, C., Maximov, T. C., Petrov, R. E. and

Andersson, P. S.: Spatial variation in concentration and sources of organic carbon in the Lena River, Siberia, J. Geophys. Res. Biogeosciences, 122(8), 1999–2016, doi:10.1002/2017JG003858, 2017.

Lammers, R. B., Shiklomanov, A. I., Vörösmarty, C. J., Fekete, B. M. and Peterson, B. J.: Assessment of contemporary Arctic river runoff based on observational discharge records, J. Geophys. Res. Atmos., doi:10.1029/2000JD900444, 2001.

Lange, S.: EartH2Observe, WFDEI and ERA-Interim data Merged and Bias-corrected for ISIMIP (EWEMBI), GFZ Data Serv., doi:10.5880/pik.2016.004, 2016.

Lange, S.: Bias correction of surface downwelling longwave and shortwave radiation for the EWEMBI dataset, Earth Syst. Dyn., doi:10.5194/esd-9-627-2018, 2018.

Laudon, H., Buttle, J., Carey, S. K., McDonnell, J., McGuire, K., Seibert, J., Shanley, J., Soulsby, C. and Tetzlaff, D.: Cross-regional prediction of long-term trajectory of stream water DOC response to climate change, Geophys. Res. Lett., doi:10.1029/2012GL053033, 2012.

Lauerwald, R., Hartmann, J., Ludwig, W. and Moosdorf, N.: Assessing the nonconservative fluvial fluxes of dissolved organic carbon in North America, J. Geophys. Res. Biogeosciences, doi:10.1029/2011JG001820, 2012.

Lauerwald, R., Laruelle, G. G., Hartmann, J., Ciais, P. and Regnier, P. A. G.: Spatial patterns in CO2evasion from the global river network, Global Biogeochem. Cycles, doi:10.1002/2014GB004941, 2015.

Lloyd, J., Shibistova, O., Zolotoukhine, D., Kolle, O., Arneth, A., Wirth, C., Styles, J. M., Tchebakova, N. M. and Schulze, E. D.: Seasonal and annual variations in the photosynthetic productivity and carbon balance of a central Siberian pine forest, Tellus, Ser. B Chem. Phys. Meteorol., doi:10.1034/j.1600-0889.2002.01487.x, 2002.

Nachtergaele, Freddy, Harrij van Velthuizen, Luc Verelst, N. H. Batjes, Koos Dijkshoorn, V. W. P. van Engelen, Guenther Fischer, Arwyn Jones, Luca Montanarella, Monica Petri, Sylvia PrielerB, Xuezheng Shi, Edmar Teixera and David Wiberg: The harmonized world soil database, Proc. 19th World Congr. Soil Sci. Soil Solut. a Chang. World, Brisbane, Aust. 1-6 August 2010, pp. 34-37., 34–37 [online] Available from: https://library.wur.nl/WebQuery/wurpubs/fulltext/154132, 2010.

Qiu, C., Zhu, D., Ciais, P., Guenet, B., Krinner, G., Peng, S., Aurela, M., Bernhofer, C., Brümmer, C., Bret-Harte, S., Chu, H., Chen, J., Desai, A. R., Dušek, J., Euskirchen, E. S., Fortuniak, K., Flanagan, L. B., Friborg, T., Grygoruk, M., Gogo, S., Grünwald, T., Hansen, B. U., Holl, D., Humphreys, E., Hurkuck, M., Kiely, G., Klatt, J., Kutzbach, L., Largeron, C., Laggoun-Défarge, F., Lund, M., Lafleur, P. M., Li, X., Mammarella, I., Merbold, L., Nilsson, M. B., Olejnik, J., Ottosson-Löfvenius, M., Oechel, W., Parmentier, F. J. W., Peichl, M., Pirk, N., Peltola, O., Pawlak, W., Rasse, D., Rinne, J., Shaver, G., Peter Schmid, H., Sottocornola, M., Steinbrecher, R., Sachs, T., Urbaniak, M., Zona, D. and Ziemblinska, K.: ORCHIDEE-PEAT (revision 4596), a model for northern peatland CO2, water, and energy fluxes on daily to annual scales, Geosci. Model Dev., 11(2), 497–497, doi:10.5194/gmd-11-497-2018, 2018.

Rawlins, M. A., Fahnestock, M., Frolking, S. and Vörösmarty, C. J.: On the evaluation of snow water equivalent estimates over the terrestrial Arctic drainage basin, in Hydrological Processes., 2007.

Reynolds, C. A., Jackson, T. J. and Rawls, W. J.: Estimating soil water-holding capacities by linking the Food and Agriculture Organization soil map of the world with global pedon databases and continuous pedotransfer functions, Water Resour. Res., 36(12), 3653–3662, doi:10.1029/2000WR900130, 1999.

Roser, C., Montagnani, L., Schulze, E.-D., Mollicone, D., Kolle, O., Meroni, M., Papale, D., Marchesini, L. B., Federici, S. and Valentini, R.: Net CO2 exchange rates in three different successional stages of the "Dark Taiga" of central Siberia, Tellus B, doi:10.1034/j.1600-0889.2002.01351.x, 2002.

Sawamoto, T., Hatano, R., Yajima, T., Takahashi, K. and Isaev, A. P.: Soil respiration in siberian taiga ecosystems with different histories of forest fire, Soil Sci. Plant Nutr., doi:10.1080/00380768.2000.10408759, 2000.

Schulze, E. D., Lloyd, J., Kelliher, F. M., Wirth, C., Rebmann, C., Luhker, B., Mund, M., Knohl, A., Milyukova, I. M., Schulze, W., Ziegler, W., Varlagin, A. B., Sogachev, A. F., Valentini, R., Dore, S., Grigoriev, S., Kolle, O., Panfyorov, M. I., Tchebakova, N. and Vygodskaya, N. N.: Productivity of forests in the eurosiberian boreal region and their potential to act as a carbon sink - a synthesis, Glob. Chang. Biol., doi:10.1046/j.1365-2486.1999.00266.x, 1999.

Serikova, S., Pokrovsky, O. S., Ala-Aho, P., Kazantsev, V., Kirpotin, S. N., Kopysov, S. G., Krickov, I. V., Laudon, H., Manasypov, R. M., Shirokova, L. S., Soulsby, C., Tetzlaff, D. and Karlsson, J.: High riverine CO2 emissions at the permafrost boundary of Western Siberia, Nat. Geosci., doi:10.1038/s41561-018-0218-1, 2018.

Shvartsev, S. L.: Geochemistry of fresh groundwater in the main landscape zones of the Earth, Geochemistry Int., doi:10.1134/S0016702908130016, 2008.

Shvidenko, A. and Nilsson, S.: A synthesis of the impact of Russian forests on the global carbon budget for 1961-1998, Tellus, Ser. B Chem. Phys. Meteorol., doi:10.1034/j.1600-0889.2003.00046.x, 2003.

Sommerkorn, M.: Micro-topographic patterns unravel controls of soil water and temperature on soil respiration in three Siberian tundra systems, Soil Biol. Biochem., doi:10.1016/j.soilbio.2008.03.002, 2008.

Tarnocai, C., Canadell, J. G., Schuur, E. A. G., Kuhry, P., Mazhitova, G. and Zimov, S.: Soil organic carbon pools in the northern circumpolar permafrost region, Global Biogeochem. Cycles, 23(2), doi:Gb2023\n10.1029/2008gb003327, 2009.

Tootchi, A., Jost, A. and Ducharne, A.: Multi-source global wetland maps combining surface water imagery and groundwater constraints, Earth Syst. Sci. Data, 11, 189–220, doi:10.5194/essd-11-189-2019, 2019.

Vonk, J. E., Mann, P. J., Davydov, S., Davydova, A., Spencer, R. G. M., Schade, J., Sobczak, W. V., Zimov, N., Zimov, S., Bulygina, E., Eglinton, T. I. and Holmes, R. M.: High biolability of ancient permafrost carbon upon thaw, Geophys. Res. Lett., 40(11), 2689–2693, doi:10.1002/grl.50348, 2013.

Vonk, J. E., Tank, S. E., Mann, P. J., Spencer, R. G. M., Treat, C. C., Striegl, R. G., Abbott, B. W. and Wickland, K. P.: Biodegradability of dissolved organic carbon in permafrost soils and aquatic systems: A meta-analysis, Biogeosciences, 12(23), 6915–6930, doi:10.5194/bg-12-6915-2015, 2015a.

Vonk, J. E., Tank, S. E., Bowden, W. B., Laurion, I., Vincent, W. F., Alekseychik, P., Amyot, M., Billet, M. F., Canário, J., Cory, R. M., Deshpande, B. N., Helbig, M., Jammet, M., Karlsson, J., Larouche, J., MacMillan, G., Rautio, M., Walter Anthony, K. M. and Wickland, K. P.: Reviews and Syntheses: Effects of permafrost thaw on arctic aquatic ecosystems, Biogeosciences Discuss., 12(23), 7129–7167, doi:10.5194/bgd-12-10719-2015, 2015b.

Vorosmarty, C. J., Fekete, B. M., Meybeck, M. and Lammers, R. B.: Global system of rivers: Its role in organizing continental land mass and defining land-To-Ocean linkages, Global Biogeochem. Cycles, 14(2), 599–621, doi:10.1029/1999GB900092, 2000.

Wang, S., Huang, J., Yang, D., Pavlic, G. and Li, J.: Long-term water budget imbalances and error sources for cold region drainage basins, Hydrol. Process., doi:10.1002/hyp.10343, 2015.

Yang, D., Kane, D., Zhang, Z., Legates, D. and Goodison, B.: Bias corrections of long-term (1973-2004) daily precipitation data over the northern regions, Geophys. Res. Lett., doi:10.1029/2005GL024057, 2005.

Ye, B., Yang, D. and Kane, D. L.: Changes in Lena River streamflow hydrology: Human impacts versus natural variations, Water Resour. Res., doi:10.1029/2003WR001991, 2003.

Ye, B., Yang, D., Zhang, Z. and Kane, D. L.: Variation of hydrological regime with permafrost coverage over Lena Basin in Siberia, J. Geophys. Res. Atmos., 114, D7, doi:10.1029/2008JD010537, 2009.

Zhang, X., Hutchings, J. A., Bianchi, T. S., Liu, Y., Arellano, A. R. and Schuur, E. A. G.: Importance of lateral flux and its percolation depth on organic carbon export in Arctic tundra soil: Implications from a soil leaching experiment, J. Geophys. Res. Biogeosciences, 122(4), 796–810, doi:10.1002/2016JG003754, 2017.